Coastal Engineering 188 (2024) 104428

Contents lists available at ScienceDirect

Coastal Engineering

journal homepage: www.elsevier.com/locate/coastaleng

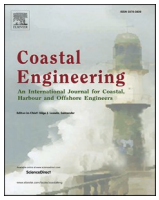

Laboratory evaluation of the effectiveness of nature-assisted beach enhancement techniques

E. Pellón *, C. Vidal, P. Gomes da Silva, I. Aniel-Quiroga, M. González, R. Medina

IHCantabria - Instituto de Hidráulica Ambiental de la Universidad de Cantabria, Santander, Spain

ARTICLE INFO

Keywords:
Working with nature
Scraping
Ploughing
Accretion enhancement
Beach widening
Reduced-scale laboratory experiments

ABSTRACT

Beaches are eroded and accrete under the effect of storms and calm marine conditions, respectively. Normally, beaches reach their narrower state in spring, after the action of winter storms. Accretion processes are slow, and maximum beach recovery doesn't occur until late summer. Sometimes this recovery is not enough to reach the width the beach had the previous year, producing a progressive shoreline retreat and an increased risk of dune erosion and inland flooding during the following winter seasons. The need for wider beaches in early summer for touristic purposes and social support to soft-engineering measures, have increased the interest in Nature-Assisted Beach Enhancement (NABE) techniques. In this study, reduced-scale laboratory experiments on beach ploughing and scraping allowed the comparison of various of these techniques and their effectiveness in controlled conditions for the first time. The beach widening and accretion achieved for five different NABE geometries were analysed and contrasted with natural (control) conditions. Our results show that the best technique is goal-dependent. For dry beach widening, ploughing is recommended as an effective and easy-to-design technique. Scraping the lower intertidal area and placing the sand on an intertidal bar or the beachfront are also effective alternatives if adequately designed. For dune nourishment, the best option is scraping the upper intertidal area and using the borrowed sand for dune regeneration. In general, all the analysed techniques enhance natural beach accretion, in collaboration with natural processes, thus reducing the human action required to achieve the desired objectives from a Building with Nature perspective.

1. Introduction

Beach erosion and coastal flooding are major concerns in coastal areas. Ten percent of the world's population lives in a nearshore region at less than 10 m above sea level (McGranahan et al., 2007). Luijendijk et al. (2018) found that 31% of the world's ice-free shorelines are sandy, and 24% of those beaches are eroding at rates exceeding 0.5 m/yr. Coastal erosion and sea level rise effects threaten an important percentage of the world's population. Progressive narrowing of dry beach width and dune deterioration increase the risk of damages to coastal areas.

Beach erosion is clearly visible during winter storms. On the contrary, accretion processes occur during calm weather periods and are slow (Gallagher et al., 1998; Yoo et al., 2021) taking several months to achieve a noticeable widening of the upper dry beach area. In locations subject to anomalous energetic winter storms, accretion processes are not enough to re-establish the original shoreline's position after winter (Gordon, 2015; Yoo et al., 2021), and progressive shoreline retreat may occur both in eroding or long-term equilibrium shorelines (that are in equilibrium when anomalous energetic winter storms do not occur).

The boom of coastal tourism in the last decades has increased the demand for wider beaches during the spring and summer seasons. Usually, in early spring, beaches are in their narrower state, due to the recent erosion produced by winter storms. It is not until late summer that accretion processes restore beaches to their wider state (Aubrey, 1979).

Coastal decision-makers demand soft engineering tools to deal with coastal erosion threats while providing beach widening for touristic purposes. In this sense, beach nourishment is a widespread measure (Hamm et al., 2002), that may provide a solution for both issues if performed in early spring. The drawback of this kind of solution lies in the difficulty to find reservoirs with appropriate sand characteristics (size, colour) and where sand dredging does not pose an environmental problem. To tackle these problems, previous studies propose the use of nature-assisted beach enhancement (NABE) techniques (Gordon, 2015). These techniques aim to accelerate the accretion processes occurring

* Corresponding author.
E-mail address: pellone@unican.es (E. Pellón).

https://doi.org/10.1016/j.coastaleng.2023.104428
Received 12 April 2023; Received in revised form 29 September 2023; Accepted 17 November 2023
Available online 23 November 2023

naturally on the beach in a Building with Nature philosophy. Specifically, two NABE techniques are analysed here: (1) beach scraping and (2) beach ploughing.

Bruun (1983) describes beach scraping as the removal of material from the lower part of the aerial beach and subsequent deposition on the upper part of the beach or at the dune's toe. This technique has been used since the 19th century, but few scientific studies have analysed its effects (Carley et al., 2010). One advantage of this technique is that the borrowed sand belongs to the same beach system and therefore its characteristics are those of the native sand, so it can be used both for dune nourishment and to generate a wider beach (Dare, 2003). However, such scraping must be done responsibly, following specific rules to avoid adverse effects on the ecosystem or adjacent beaches (Bruun, 1983). For example, the recommended maximum depth of the borrow area is 0.3 m for fine sand beaches, and the volume must not exceed natural accretion rates integrated over the whole summer season (McNinch and Wells, 1992; Tye, 1983) to allow the beach to recover. An additional interesting statement about beach scraping is that it accelerates natural beach accretion (Smutz et al., 1980), capturing more sand from the offshore part of the beach profile that moves naturally to the upper part of the intertidal region or beachfront. This Building with Nature strategy allows the mobilization of a larger volume of sediment with fewer human actions (less cost and less ecosystem disturbance). Carley et al. (2010) and Smutz et al. (1980) state that removing the borrowed sand turns the beach profile flatter or more dissipative, augmenting the disequilibrium between the scraped profile and the equilibrium profile of low energy waves, thus increasing the associated accretion. This is the main reason why scraping is also called nature-assisted beach enhancement although, to date, no field or laboratory study supports this statement.

Beach ploughing is an innovative technique that consists of mechanically ploughing the intertidal area of a beach by terrestrial means during low tide. Ploughing is expected to modify marine dynamics in the intertidal area and accelerate beach accretion. It is also presented as a nature-assisted beach enhancement technique. Monge-Ganuzas et al. (2017) applied ploughing for the first time at Laida beach (northern Spain). The intertidal area of Laida beach was ploughed 22 times, between July and September 2015, generating ridges and furrows with a length of 1.42 m and a height of 0.27 m (right panel of Fig. 4). Gainza et al. (2019) analysed the evolution of the beach and found that ploughing accelerated natural onshore bar migration. Given these promising results, Pellón et al. (2023) performed laboratory experiments to analyse ploughing effectivity under controlled conditions. They compared the accretion between a natural intertidal segment of a beach profile and a ploughed one, both at a real scale. The comparison was performed for seven different tidal levels and the same accretive wave conditions during 1 h. The main results indicated that ploughing generates extra bottom roughness of the intertidal bottom, which leads to extra wave dissipation and accretion enhancement. Pellón et al. (under review) extended this analysis to longer-duration tests. The results showed that ploughed bedforms migrate onshore while adopting a softened form as waves act on the ridges and furrows. The artificially generated bedforms enhanced accretion during the first 2–3 h of wave action, after which they almost disappeared. The cumulative effect of repeating beach ploughing at every low tide and the combined effect of waves and tides on the whole beach profile are key factors to quantify the success of ploughing as management option. None of these factors have been considered in previous studies, and will be analysed here for the first time.

Few laboratory experiments have been performed on soft-engineering techniques. Larsen et al. (2023) presented a review of laboratory studies about beach nourishment, but most of them analysed nourishment of the submerged part of the beach profile (bar or through) and therefore their findings do not apply to assessing beach scraping or beach ploughing techniques. Alsina et al. (2012), conducted large-scale experiments and assessed bar migration with two different beachfront morphologies. This morphology can be considered as the reshaping that would be applied in tideless beaches (it only affects the aerial part of the beachfront). The results showed that the bar had a greater tendency to accrete when the beachfront was more dissipative. Sánchez-González et al. (2017) performed large-scale laboratory experiments on beach scraping with the combined effect of waves and tides. They analysed the suitability of two different filling locations for the particular conditions of Orzán and Riazor beach (A Coruña, Galicia). This beach is composed of medium-coarse sediment and present a beach profile shape that is not commonly observed in other beaches. Therefore, the results cannot be extrapolated to places with different characteristics. Additionally, Sánchez-González et al. (2017) described the experimental layout, but the results and main conclusions extracted from their research have not been published yet, and therefore cannot be compared to the ones obtained here.

The aim of this study is to investigate the strenghts and weaknesses of NABE techniques to enhance beach natural recovery. To achieve this goal, we present an analysis of the effect of beach scraping and ploughing based on reduced-scale laboratory experiments. The experiments were conducted to consider the simultaneous effect of waves and tides on a fine sand beach. To the authors' knowledge, this is the first time that beach scraping is assessed under these conditions in the laboratory, allowing the validation of Carley's et al. (2010) and Smutz's et al. (1980) statements that scraping enhances beach accretion. We also compare beach scraping effectiveness with natural and ploughing behaviour. The document is structured as follows: The laboratory experiments scaling design and setup are described in section 2. The results are shown in section 3 and discussed in section 4. Finally, section 5 presents the main conclusions.

2. Laboratory experiments description/methodology

Reduced-scale laboratory experiments were performed at the Directional Wave Tank (Tanque de Oleaje Direccional, TOD, in Spanish) at IHCantabria's facilities. The beach profile was reproduced with low-density synthetic sediment to reduce scale effects on sediment transport processes. Both techniques, scraping and ploughing were analysed under three different accretive wave conditions including simultaneous tide simulation. In this section, the scaling design and the experimental setup are described.

2.1. Scaling design

Movable-bed, reduced-scale laboratory modelling is still a challenge. Reproducing all the dimensionless parameters that determine coastal hydrodynamics and sediment transport at these reduced scales has not been achieved yet. The state-of-the-art covers two approaches: (1) the use of real sediment with the same density as in nature, and (2) the use of low-density synthetic sediment. The use of real sediment makes scale effects inevitable, and some authors do not even indicate a scale or prototype (Baldock and Alsina, 2013; Guannel et al., 2007; Larsen et al., 2023). Sánchez-González et al. (2017) scaled sediment grain size to reduce scale effects in the breaking zone. Few studies use low-density sediment although it allows the similarity between 4 out of 5 of the desired dimensionless parameters. The use of low-density materials reduces scale effects but should be designed with care and is costly. Different approaches can be followed, such as the one proposed by Grasso et al. (2009) or the methodology described in Appendix I. The advantage of the methodology proposed in Appendix I is that the calculations can be made with simpler expressions.

The length scale used for the calculations of the experiments conducted in this study, $\lambda_l = 8$ was determined by the capabilities and size of the wave tank where the model was built. The details of the calculations are given in Appendix I, where Table 3 summarizes the known parameters, the target values for the sediment characteristics (among others), and the resulting values and scales of the relevant parameters.

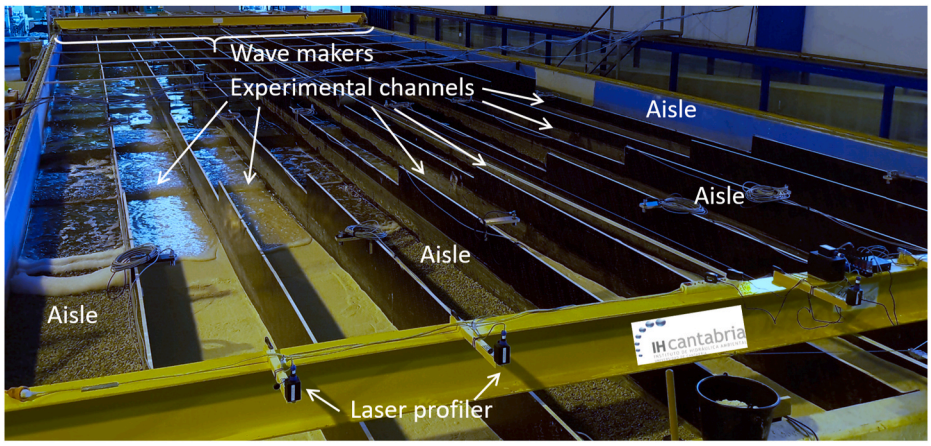

Fig. 1. Directional Wave Tank (TOD) during the experiments.

The density of the sediment used for physical models is restricted by the densities of available materials. In this study, we used a synthetic sediment which was very similar to the targeted one (i.e. plastic blast of density $\rho_s = 1\ 500\ kg/m^3$, gradation 40/60, mean grain size $d_{50} = 0.37$ mm, and porosity of 0.5, see Table 3 of Appendix I). With this sediment, all parameters (Froude, Shields, Reynolds grain and Rouse) were similar in the prototype and the model. The dimensionless fall velocity however was higher in the prototype than in the model, meaning that the modelled beach would tend to be more reflective than the prototype (see more details on the implications of a higher dimensionless fall velocity in Appendix I).

The scaling analysis was performed for the design of the experiments. Nevertheless, the experimental results shown here are not seen as a model scale version of a prototype scale.

2.2. Experimental setup

The experiments were carried out in the Directional Wave Tank (TOD) at IHCantabria's facilities. The TOD (see Fig. 1) is 28 m long, 8.6 m wide, and 1.2 m high. The tank was divided longitudinally into 10 channels, six of them were used to test different nature-assisted beach enhancement (NABE) techniques under the same marine dynamics, and the remaining four were used as aisles to access the testing profiles while scraping and ploughing. Each channel was 0.8 m wide, minimizing boundary effects, with a cross-channel standard deviation of the geometry below 0.01 m on the whole beach profile, and below 0.001 m on the beachfront (characterized by 3D laser scanner measurements randomly realized). On the central part of each channel, geometric measurements were taken every low tide with a laser profiler with horizontal and vertical precision of 0.002 m.

Experimental channels were filled with low density ($d_{50} = 0.37$ mm and $\rho_s = 1\ 500\ kg/m^3$) synthetic sediment to reduce scaling effects (see previous section). The sediment was placed with an initial uniform slope of 1/21, and two tidal cycles of slightly energetic waves ("pre-test waves", Table 1) were simulated to obtain a dissipative beach profile which is typical in spring, at the beginning of the good weather season (Fig. 2). Then, the marine climate of each Test (A, B, or C, see Table 1) was simulated until the maximum accretion on the beachfront was reached. At least one tidal cycle more than the one shown here was simulated for each Test, which allowed the verification that the maximum accretion had been achieved. The waves simulated during the Tests were low energetic, typical of spring and summer marine conditions. This process was repeated for each Test, manually restoring the sediment layout with a uniform slope of 1/21 after them, which ensured the same initial conditions for each Test. The thickness of the synthetic sediment layer varies between 0.1 and 0.25 m depending on the cross-shore position and the Test. The "pre-test waves" simulation was used to check the repeatability of the experiments. Two tidal cycles of "pre-test waves" were not enough to achieve an equilibrium profile, but were considered enough to reach a dissipative profile typical of spring. The geometry of this initial profile was equal for all channels, and therefore a comparative analysis could be performed. Four channels lying between the test-channels were used as working aisles (so as not to tread on the experimental channels) and filled with gravel with the same uniform slope to avoid wave reflections.

Three Tests were simulated (A, B, and C) with different wave characteristics, all of them ensuring that accretion was produced ($\Omega < 2.4$, indicating highly probable accretion according to Kraus et al. (1991), see Table 1). All the simulations included a simultaneous sea level variation according to a semidiurnal tide (4 h duration, approximately Froude scaled) with 0.3 m of tidal range for Test A and 0.2 m for Test B and C. The bottom of the channel next to the wave generators was 0.4 m below the low tide level for all Tests. Pre-test waves were run before each Test, with the same tidal range as that of their corresponding Test, to achieve the initial profile (a dissipative profile generated with waves with $\Omega > 4$). Test C waves were small enough to test the lower limit of accretion that can be produced with natural waves but also had similar Ω parameter to Test A for comparison. The wave characteristics were

Table 1
Model and prototype marine dynamics simulated.

Wave config.	Model				Prototype			
	H_{sm} (m)	T_{pm} (s)	$Tide_m$ (m)	Ω_m	H_{sp} (m)	T_{pp} (s)	$Tide_p$ (m)	Ω_p
Pre-test A	0.19	2.23	0.30	4.24	1.54	6.30	2.40	7.78
Pre-test B	0.19	2.24	0.20	4.09	1.49	6.35	1.60	7.50
Pre-test C	0.18	2.29	0.20	3.88	1.44	6.48	1.60	7.12
Test A	0.06	2.93	0.30	1.01	0.48	8.28	2.40	1.85
Test B	0.04	2.96	0.20	0.69	0.33	8.38	1.60	1.27
Test C	0.03	1.64	0.20	0.97	0.26	4.64	1.60	1.78

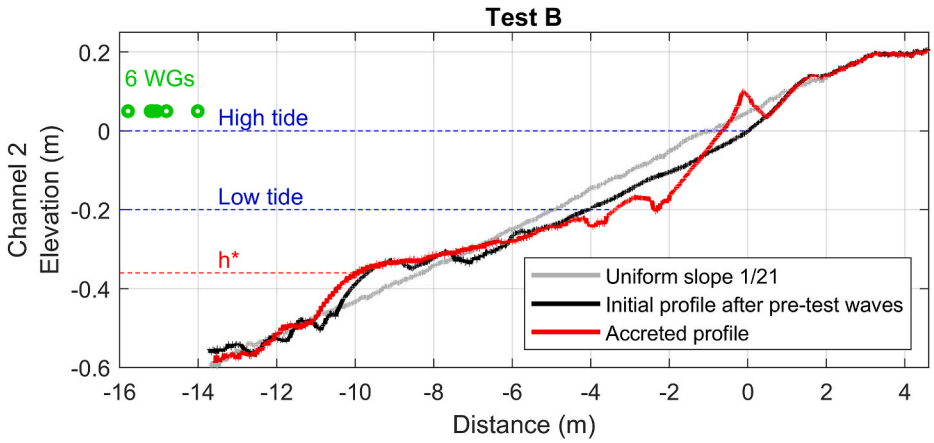

Fig. 2. Setup, initial profile, and maximum accretion achieved for Test B at prototype scale. h* is the depth of closure for test waves. Green circles show the position of the free surface sensors (WGs). The bottom of the tank was at −0.6 m.

Table 2
Characteristics of the NABE technique conducted in each channel.

	Acronym	Technique	Borrow area	Filling area
Channel 1	PLOUGH	Ploughing	Ridges and furrows	
Channel 2	NAT	Natural	No sand movement – Control	
Channel 3	L2B	Scraping	Lower intertidal	Intertidal bar
Channel 4	L2BF	Scraping	Lower intertidal	Beachfront
Channel 5	L2D	Scraping	Lower intertidal	Dune or upper dry beach
Channel 6	U2D	Scraping	Upper intertidal	Dune or upper dry beach

measured by 6 capacitive wave gauges (WGs) that recorded the free surface elevation at 50 Hz (see sensors location in Fig. 2). Other sensors were installed for the control of the experiments (2 additional capacitive WGs, 12 ultrasonic WGs [2 on each channel], top view images every minute, and 3D laser scanners) Table 1 shows the model and prototype wave and tide characteristics of each Test. The wave spectrum used was JONSWAP (Hasselmann et al., 1973) for Test waves and TMA (Hughes, 1984) for pre-test waves. The reflection coefficient for pre-test waves oscillates between 0.15 and 0.18, and the coefficient for Test waves oscillates between 0.15 and 0.23.

These marine dynamics affect the six channels filled with synthetic sediment equally. Each of them was used to test a different NABE technique. Table 2 summarizes the characteristics of the techniques tested on each channel. Channel 2 was used as control, with no NABE applied, and represents the natural evolution of the beach. Ploughing was applied in the intertidal area of Channel 1 every low tide. Scraping was applied in Channels 3 to 6, with different locations of the borrow and filling areas. The borrow area was 0.25–0.3 m deep (as recommended by Carley et al., 2010) and had 11.2 m of cross-shore extent at the prototype scale (0.03 m deep and 1.4 m cross-shore at model scale). This means that around 3 m^3 of sediment were mobilized per meter of beach (0.045 m^3 at model scale).

Fig. 3 shows the ploughing and scraping borrow and filling areas for each channel. The borrow area was the low intertidal part of the beach profile for Channels 3, 4, and 5, next to the low tide limit to perform the scraping by terrestrial machinery. In Channel 6 the borrow area was the upper part of the intertidal area, just below the high tide level. All this sediment was placed on an intertidal bar in Channel 3, on the beachfront for Channel 4, and on the dune (taken out of the experimental tank) for Channels 5 and 6. The sand extracted from those channels for dune nourishment was placed back in the next Test to ensure the same amount of sand.

The left panel in Fig. 4 displays a zoom of the ploughing area shown in the top-left panel of Fig. 3. Ploughing was designed to be performed by a ploughing tractor at a prototype scale. This machinery can perform ridges and furrows on the sand with a wavelength of ~1.5 m and an amplitude of ~0.25 m. Therefore, the plough performed in the laboratory (model scale) had a wavelength of 0.18 m and an amplitude of 0.03 m. Ploughing was conducted from the lower part of the intertidal area, next to the low tide level, to the upper part of the intertidal zone. The tidal range was larger for Test A, and therefore the cross-shore extent of the ploughing area was 5 m for Test A and 2.5 m for Tests B and C (both at model scale), corresponding to 28 and 14 ridges and furrows, respectively.

3. Results

This section shows the results obtained from the laboratory experiments. The analysis was based on the geometry of the beach profile measured at each low tide during the experiments. This section shows (1) the formation of the beach berm during calm wave conditions, (2) an analysis of the degree of widening of the dry beach and the geometric characteristics of the berm at the maximum accretion state achieved, and (3) the study of the accretion volume. These results allow the comparison among NABE techniques and the analysis of their effectiveness in terms of widening of the dry beach area and accretion enhancing. All the results shown in this section are presented at the model scale.

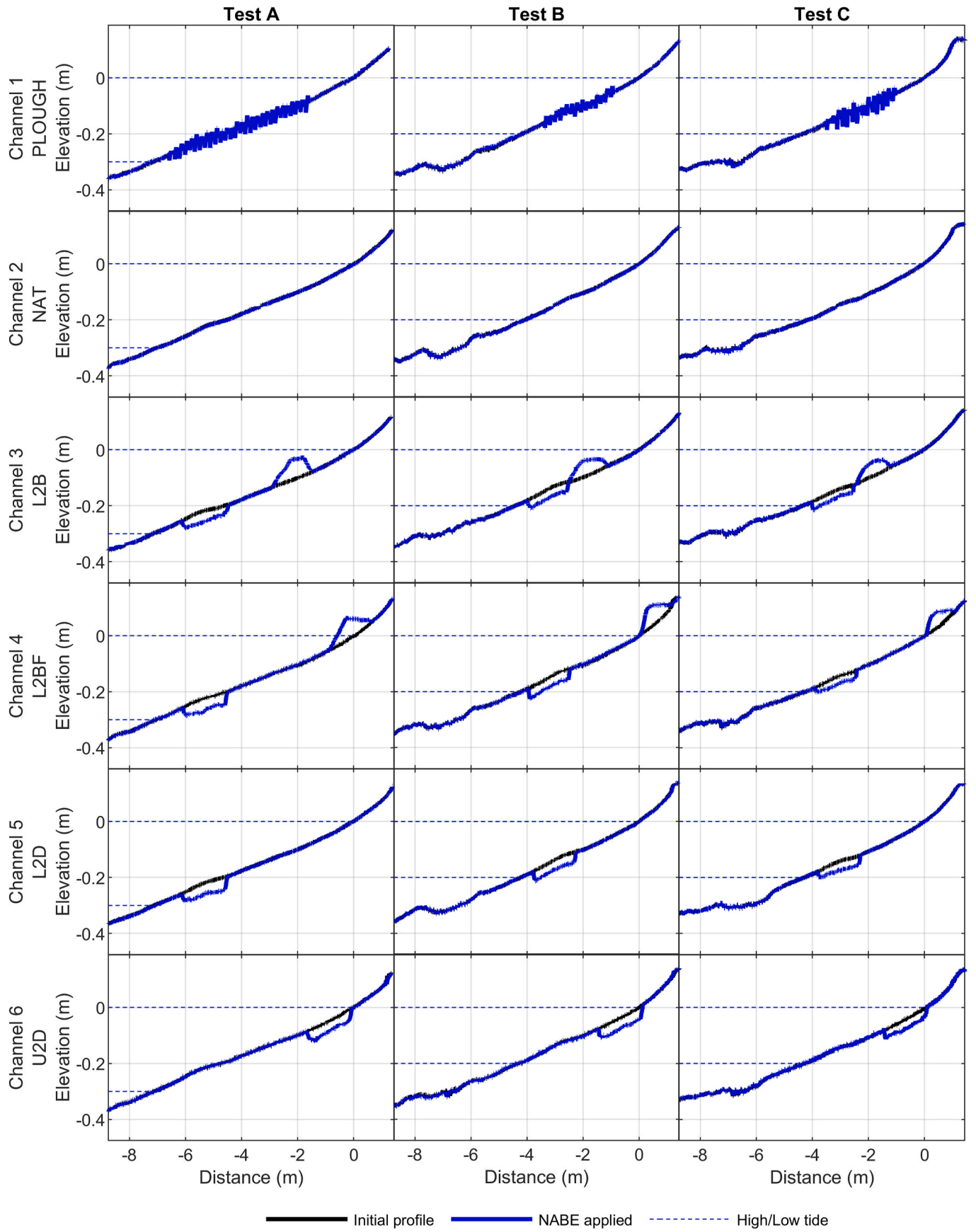

Fig. 3. NABE techniques applied to each channel and Test. Borrow and filling locations for scraped channels (3–6) and ploughing extent (channel 1).

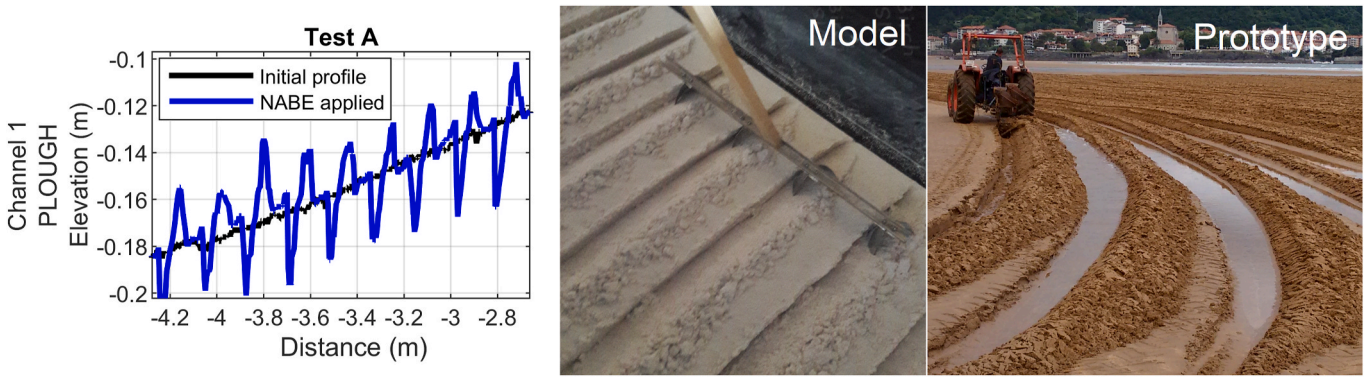

Fig. 4. Ploughing. Left: Zoom of a profile of the ploughing performed in Channel 1. Centre: Picture of ploughing being conducted at the model at a reduced scale. Right: Example of ploughing at prototype scale at Laida beach (Source: Gainza et al., 2019).

3.1. Beach berm formation

Fig. 5 shows the beach profile's evolution for each Test and channel. Fig. 6 shows a zoom-in of the beach profile around the high tide level, showing the beach berm's formation. Each panel of both figures shows the beach evolution, including the initial profile obtained after the simulation of the pre-test waves, the initial profile after NABE techniques were applied, and the maximum accretion achieved on the beach berm. The high tide, setup, and runup levels are also presented for reference. The setup ($\overline{\eta}$) and runup (R_2) levels were computed with Stockdon's et al. (2006) formulas, as shown in equations (1) and (2), respectively.

$$setup = \overline{\eta} = 0.35\beta_s (H_0 L_0)^{0.5} \tag{1}$$

$$runup = R_2 = 1.1\left(0.35\beta_s (H_0 L_0)^{0.5} + \frac{\left(H_0 L_0 \left(0.563\beta_s^2 + 0.004\right)\right)^{0.5}}{2}\right) \tag{2}$$

where β_s is swash zone slope, H_0 is deep-water wave height, $L_0 = gT^2/2\pi$ is deep-water wavelength and T is wave period. In this study, the following approximations were considered; $T = T_p$ and $H_0 = H_s$. The swash zone slope (β_s) was computed as the slope of the final beach profile of maximum accretion (red line in Figs. 5 and 6) at high tide level, considering a range of $\pm 0.8\ H_s$ around high tide level, where the beach slope was quite uniform. Only the slope at high tide was considered, as it determines the wave runup at high tide and consequently the berm's height. The tidal ranges in this experiment were meso-tidal (tidal range of 2–4 m in prototype; Short, 1991), and therefore the waves only reached the berm during high tide (but not during the falling, rising, and low tides).

A berm was observed in the final beach profile for all Tests and in all channels. There was a resemblance in the shape of the final berm of all channels in each Test (A, B or C). This indicates that the NABE technique used does not determine the geometry of the berm. On the other hand, the shape of the berm was different among Tests carried out in the same channel. The berm's height and slope at the beachfront changed according to marine dynamics, as shown in the following section.

3.2. Dry beach widening and accreted berm characteristics

Shoreline progradation was computed as the difference between the shoreline's position at the beginning of the test, and at the moment of maximum accretion. Shoreline position was taken as the point where the profile elevation is equal to the high tide plus wave setup levels. The setup level was estimated by Stockdon et al. (2006) formulation. The shoreline progradation measurement indicates the beach width increment due to sand accretion on the berm and it is indicative of the dry beach gain achieved.

Berm height was directly measured on the beach profiles as the highest point of the berm and referred to high tide level. Fig. 6 shows that the berm height achieved at the maximum accretion state was close to that of the runup level. During the experiments, the highest waves overtopped the maximum height of the berm during high tide. The sediment load carried by the waves during these events was discharged on the top of the berm making it progressively higher (see for instance the sand layer accumulated on top of the berm between −0.13 and 0.08 m cross-shore in Fig. 6e; the height step observed at 0.08 m indicates the onshore limit reached by wave overtopping). Fig. 7 shows a scatter plot of berm height and shoreline progradation for each Test. Dashed lines act as a reference of the characteristics of the berm under natural conditions (Channel 2). The empty marker shows the characteristics of the berm formed artificially by the "machinery" during the L2BF scraping of Channel 4. The berm height achieved by all the NABE experiments was similar to the naturally formed one. The height varied mainly between Tests, which means that the different incoming wave conditions were responsible for this variation but not the NABE techniques used. In Channel 4, when the artificially generated berm's height was not equal to the height of the naturally formed berm, it changed under wave action (Fig. 6j, k and l). In Test A, the artificial berm was lower than the equilibrium one, and therefore wave overtopping was produced during high tide. Those waves progressively moved the sand from the beachfront to the upper part of the berm (Fig. 6j), generating a retreat of the shoreline and a higher berm. In Tests B and C, the height of the artificially created berm was higher than the natural one, and therefore the upper part of the scraped sand was not necessary for protection during summer conditions. In these cases (Channel 4 – L2BF, Test B and C, Fig. 6k and l, respectively) a new and shorter berm was formed seaward of the position of the artificially created one with the new sediment accreted through wave action.

The final shoreline progradation achieved due to beach ploughing (Channel 1) was between 4.32% and 37.35% larger than in natural conditions for all Tests (mean of 23.41%). These results indicate that ploughing is an innovative and effective technique for beach accretion enhancement. The effect of beach scraping on shoreline progradation depended on the location of the borrow and filling areas. Channel 3 (L2B) showed an enhanced shoreline progradation compared to natural conditions between 6.79% and 63.26% (mean of 25.76%). The initial position of the shoreline in Channel 4 (after L2BF beach scraping) ranged from shorelines located landward to shorelines located seaward of the final shoreline position achieved under natural conditions (from 65.43% less to 110.84% more progradation in comparison to the profile with no NABE applied). Wave action modified the shape of the berm and the final shoreline progradation ranged between 24.07% less and 81.93% more (mean of 38.33%) than natural progradation. In this Channel 4, shoreline progradation did not exceed the natural one only for Test B, where the artificially created shoreline progradation

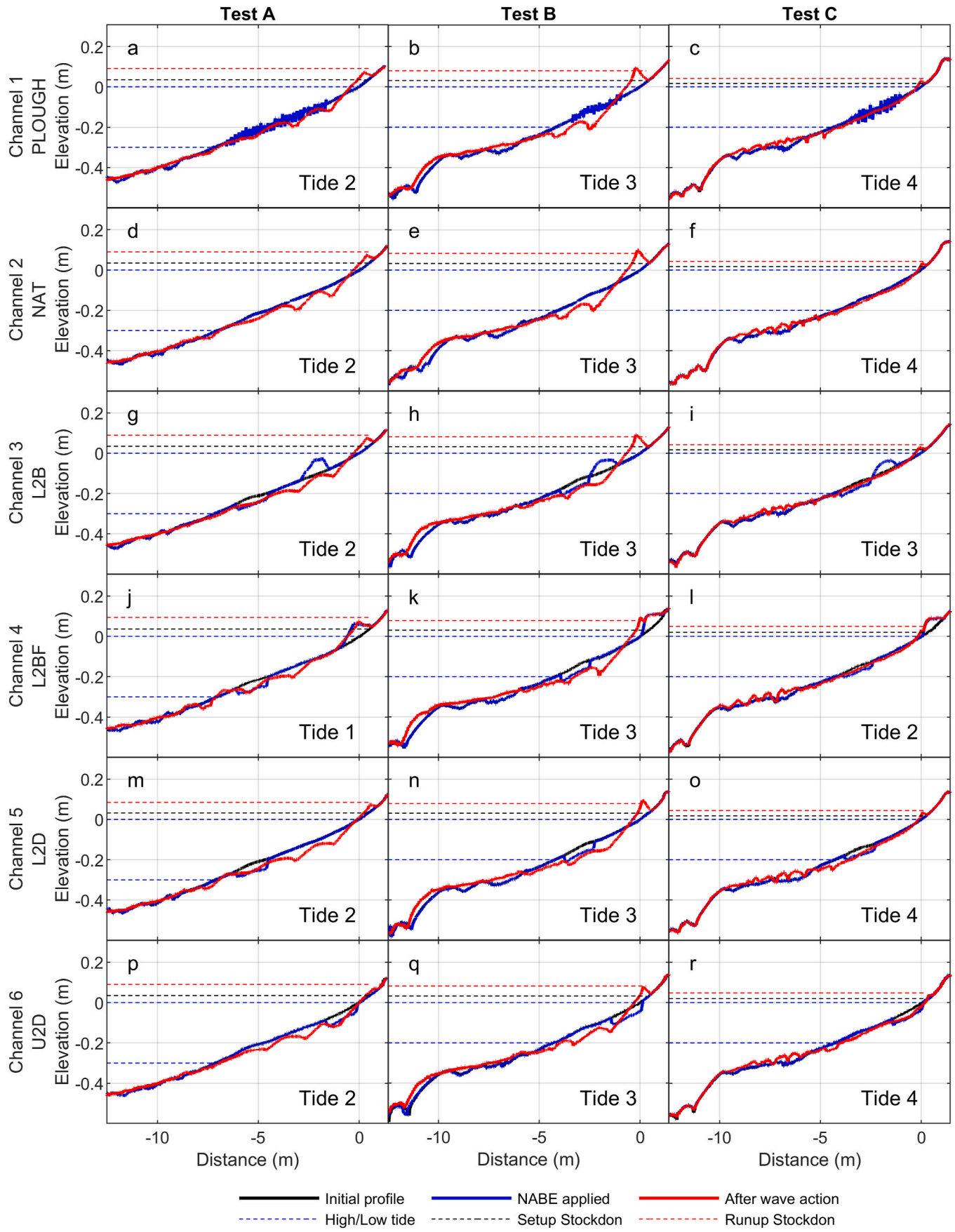

Fig. 5. Profile evolution up to the maximum accretion achieved at the beachfront. Each graph indicates the number of tidal cycles that were necessary to achieve the maximum accretion.

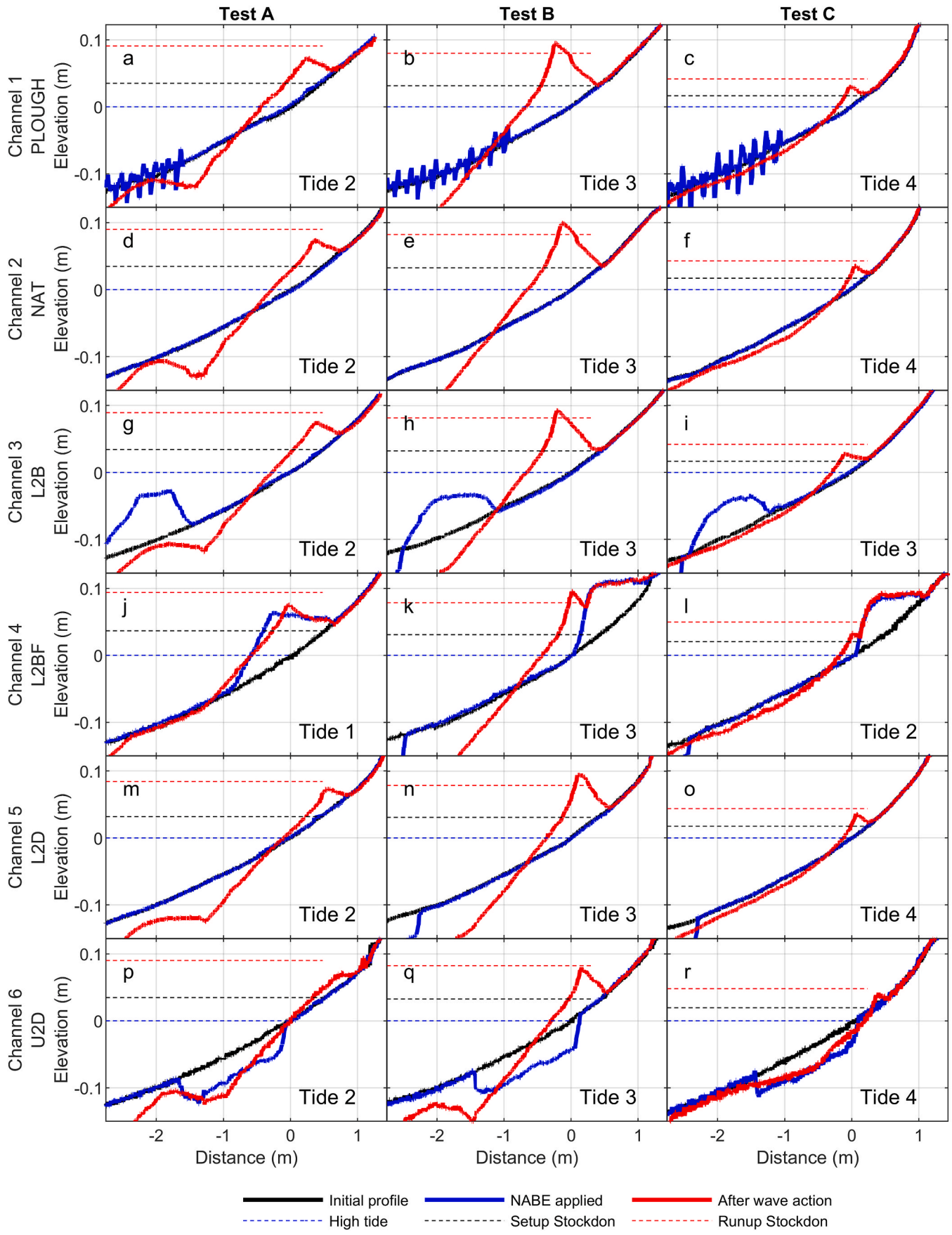

Fig. 6. Zoom-in of Fig. 5. Profile evolution up to the maximum accretion achieved at the beachfront. Each graph indicates the number of tidal cycles that were necessary to achieve the maximum accretion.

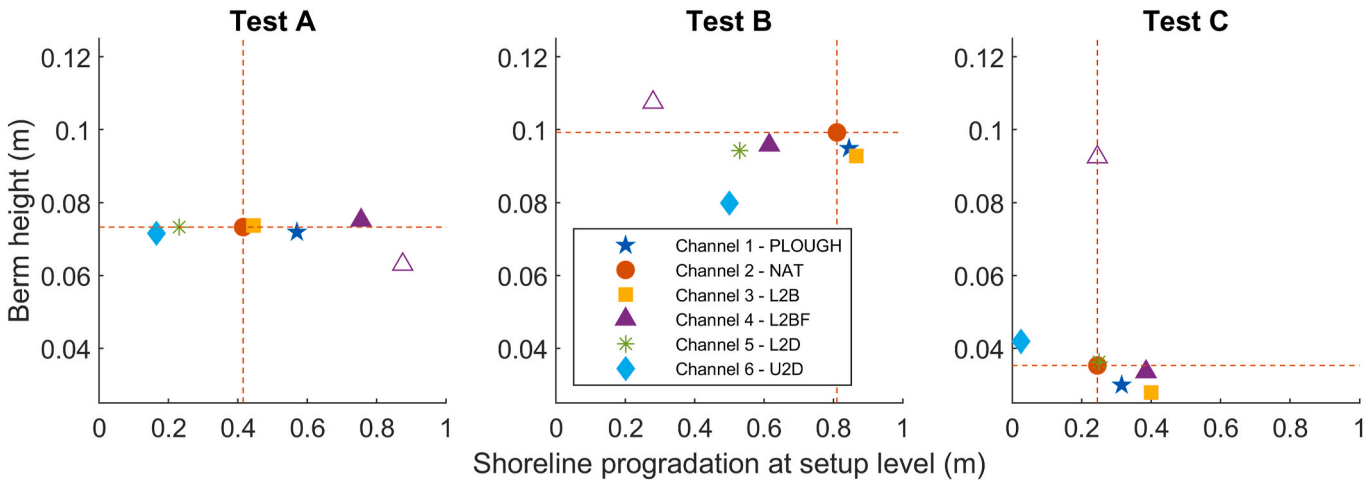

Fig. 7. Berm height and shoreline progradation achieved at maximum accretion. Dashed lines are plotted as a reference of the natural behaviour of the beach. The empty marker indicates the characteristics of the artificial berm created by scraping Channel 4.

retreated considerably compared to the expected final natural shoreline's position. In this case, the reduced amount of sediment due to removing sand and not using it to artificially induce shoreline progradation prevented the waves to produce the desired accretion. A similar scenario was found for Channels 5 and 6 (L2D and U2D respectively). In both Channels there was a lack of sediment on the active beach profile due to the volume of sand removed from the borrow area and placed on the dune (out of the area of wave action during summer). L2D achieved a final shoreline progradation between 44.58% less and 2.04% more (mean of 25.70% less) than under natural conditions. U2D showed shoreline progradations that were smaller than under natural conditions in all Tests, with values ranging between 38.27% and 89.80% less (mean of 62.77% less).

Fig. 8 shows the swash zone slope (β_s, the same used for runup calculation, see how it was computed in section 3.1) obtained for each Test and channel as a function of the shoreline progradation previously described. As with berm height, the swash zone slope only varied among Tests but not among Channels. This means that the swash zone slope was also determined by marine dynamics, while NABE techniques did not affect the final accreted equilibrium geometry. The empty marker shows the swash zone slope of the artificially generated beach berm in Channel 4 during the L2BF scraping operations. As berm height, the swash zone slope also changed toward the equilibrium slope of the accreted berm under wave action.

In Fig. 8 the black dot next to the vertical axis of each graph indicates the initial swash zone slope and shoreline progradation (0 m because it is the reference) of the pre-test waves profile. The slope was around 0.67 for all Tests, which is typical of an intermediate beach. After the low-energy wave action, the swash zone became steeper, with slopes between 0.10 and 0.15, which is common for reflective beaches.

3.3. Accreted volume

The volume of sediment accreted on the beach berm was measured by integrating the area between the initial profile obtained after the pre-test waves and the profile corresponding to the maximum accretion achieved. Only positive accretion areas around the beach berm were considered, which means from −1.5 m to 1.25 m cross-shore (i.e. from the dry beach to around 0.09 m below high tide level). For Channels 4 and 6 (L2BF and U2D), due to the location of the filling and borrow areas, the profile in which the NABE technique was applied was also considered for volume calculation. Therefore, two volume calculations were obtained for Channels 4 and 6, one referred to the pre-test waves profile and the other to the profile obtained after NABE techniques were applied. Fig. 9 shows the results obtained for each Test and channel.

Channel 2 shows the natural behaviour of the beach. In such natural conditions, the accreted volume varied depending on the different marine dynamics simulated. The largest accretion volume was obtained for

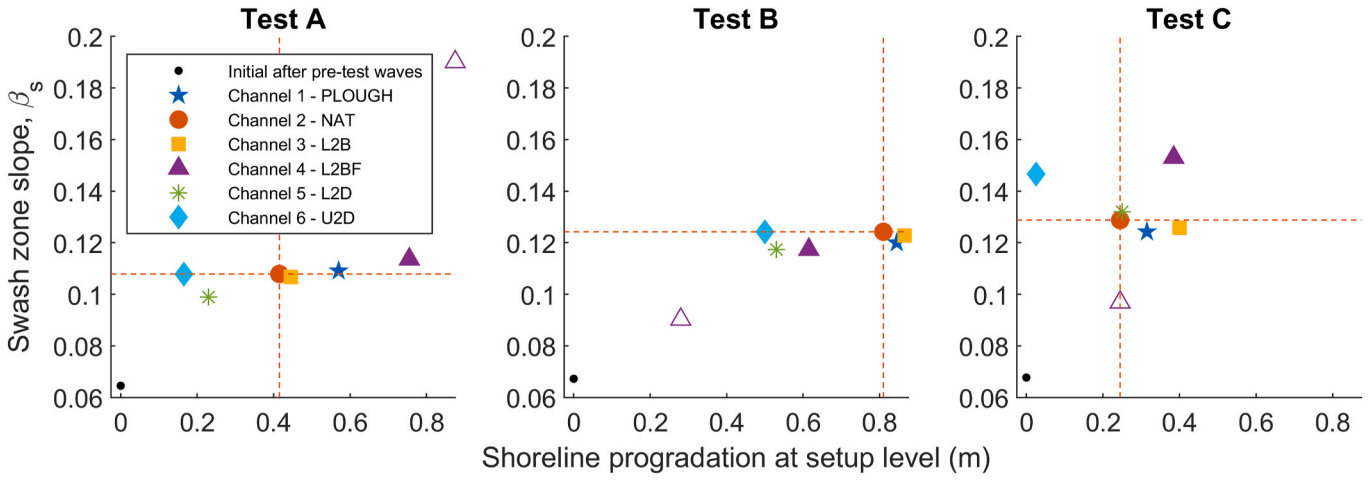

Fig. 8. Swash zone slope and shoreline progradation achieved at maximum accretion. Dashed lines are plotted as a reference of the natural behaviour of the beach. Empty markers indicate the characteristics of the berm created artificially by scraping Channel 4.

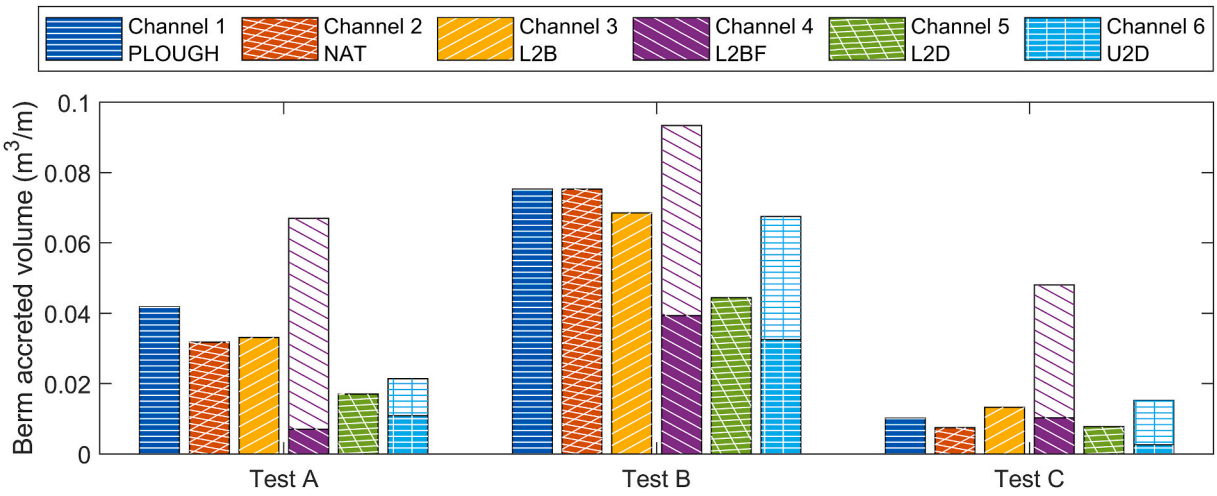

Fig. 9. Maximum accreted volume on the berm. The bar for Channel 4 shows the volumes of sediment manually mobilized by scraping (white fill with purple descending lines legend on top of purple bars) and by wave action (purple fill) filling the berm. The bar for Channel 6 represents all the volume mobilized by wave action, including the volume of sediment on the berm (blue fill) and the volume of sediment that filled the borrow area partially next to the high tide level (white fill with blue cross-squared legend on top of blue bars).

Test B, which had the lowest dimensionless fall velocity (Ω), indicating more reflective conditions (the lower the dimensionless fall velocity, the higher the beach slope). Test A and C had similar Ω (higher than Test B) and achieved lower accretion volumes, as expected. Although the dimensionless fall velocity was similar for both Tests, in Test C wave height and peak period were lower, as well as sediment transport capabilities, resulting in a smaller accreted volume. These considerations were also valid for all the other channels that had undergone the same simulated wave conditions.

The ploughing technique was tested in Channel 1. The accreted volumes obtained were 31.79% and 37.62% larger than the control for Test A and C respectively, and equal to the control for Test B. This demonstrates that the ploughing technique can enhance beach accretion by achieving a larger accreted volume of sediment and a wider dry beach (as shown before).

Channel 3 tested a scraping technique that moved the sediment from the lower intertidal area to an intertidal bar (L2B). The accreted volume was 4.23% larger than the control for Test A, 8.90% smaller for Test B, and 56.21% larger for Test C. The three Tests showed more shoreline progradation than the control. Test A and B showed similar accreted volumes to Channel 2, while the additional shoreline progradation was 7.23% and 6.79%, respectively. Besides, Test C achieved an additional 63.27% shoreline progradation, which agrees with the extra 56.21% accreted volume. The filling volume on the intertidal bar was around 0.045 m^3/m, a value larger than the accreted volume for Tests A and C. This means that for these Tests, part of the sand from the bar was moved offshore by the waves.

The L2BF beach scraping that moved the sediment from the lower intertidal area to an artificially created beach berm was carried out in Channel 4. In this case, the final berm was composed of both the artificially moved sand and the naturally accreted sediment due to wave action (see both components represented by the purple bars in Fig. 9). In all Tests, the final berm volume was larger than the control one (110.68% for Test A, 21.55% for Test B, and 491.26% for Test C), although the naturally accreted sediment volume was smaller than the control in all tests (77.75% in Test A, 50.89% in Test B, and 26.36% in Test C). It is remarkable that the amount of artificially moved sediment (around 0.045 m^3/m) was larger than the naturally accreted sediment volume for Tests A and C in the control profile. This fact can be related to the low portion of sediment that was accreted by waves in those Tests, which was 10.56% of the volume of the final berm for Test A and 12.46% for Test C, respectively. The required sand volume to form the berm was already moved by the "machinery" and therefore natural accretion only moved the sediment required to reach the final equilibrium geometry according to the swash zone slope and berm height that matched the simulated waves. In Test B, the artificially moved sand volume was lower than the volume of the berm of the control profile. In this case, the waves were able to mobilize 40.41% of the total berm volume of Channel 4. Despite that, shoreline progradation in Test B was smaller than in the control. Altogether, the scraped sediment deposited on the beachfront was not eroded by wave action, and an additional natural accretion occurred. Therefore, the L2BF scraping technique was efficient to increment dry beach sand volume, which may act as backup for winter storms.

Channel 5 (L2D) shows the results of scraping the sediment from the lower intertidal area and taking it out of the summer's wave action area (sand used for inland operations to nourish the dune or the upper part of the dry beach). In this case, the accreted volume was 46.44% smaller than the control for Test A, and 40.92% smaller for Test B. Both Tests showed smaller shoreline progradations than the control. In Test C, the accreted volume was 4.22% larger than the control, corresponding to an extra 2.04% of shoreline progradation achieved. Note that for all Tests, the volume of sand that was removed from the active beach profile was around 0.045 m^3/m (taken from the borrow area, not showed in Fig. 9), which, summed to the naturally accreted volume, exceeded the accreted volume in the control. Therefore, a larger volume of sand was recovered from the lower part of the beach profile and deposited on the beachfront and on the artificially nourished area to act as a buffer for winter erosion.

The location of the borrow area was the same (the lower intertidal area) for Channels 3, 4, and 5 (L2B, L2BF and L2D scraping techniques). However, the final volume accreted due to wave action was different, with more accretion occurring in L2B, followed by L2D, and finally L2BF. These differences can be explained by the fact that L2B had more volume of sand available in the active beach profile (the filling area was an intertidal bar). In the other two, the sand was moved completely (L2D) or partially (L2BF) out of the area affected by waves. It is noteworthy that the lowest natural accretion was achieved when filling was performed on the beachfront (L2BF). This may be due to the more reflective beach profile geometry created when filling the berm. Such reflective conditions reduced the disequilibrium between the equilibrium and the actual beach profile and, consequently, reduced sediment transport. The Tests performed for L2BF resulted in wider dry beaches than L2D but a smaller volume of sediment in the upper beach, which

reduces the protection capacity during eventual erosive winter storms.

As in Channel 5 (L2D), in Channel 6 (U2D) the sediment was also extracted from the area under the effect of summer waves but was borrowed from the upper intertidal area, next to the high tide level. In this case, the accreted sediment partially filled the borrow area. Therefore, the berm's accreted volume was composed of the sum of the sediment that filled the borrow area and the sediment accumulated on the initial beach profile (without using NABE). Fig. 9 shows both components. The accreted volume was 32.68% smaller than the control in Test A, 10.33% smaller in Test B, and 106.18% larger in Test C. A considerable amount of this sediment filled the borrow area: 48.98% of the accreted volume in Test A, 51.86% in Test B, and 83.25% in Test C. As a consequence, the volume that generated a new berm and produced shoreline progradation was lower than the control for all Tests, matching the results of less shoreline progradation presented before. In fact, U2D showed the most retreated shoreline positions at the end of the experiments, although the total amount of sediment captured from the lower part of the beach profile was the largest one of all channels (taking into account the volume accreted by waves and the 0.045 m^3/m extracted from the borrow area). By comparing the results from L2D and U2D, it can be stated that sand extraction from the upper intertidal area leads to more accretion on the beach profile due to the generation of a more dissipative beach profile geometry, as suggested by previous authors.

4. Discussion

NABE techniques are widely applied on many beaches, although their actual effect on beach accretion had not been checked until now. The design of NABE techniques should match the aim of the project (Carley et al., 2010), and take into consideration local marine and aeolian dynamics, as well as ecological concerns. The recommended maximum depth of the borrow area to be scraped is 0.3 m for sandy beaches (Bruun, 1983) and the volume should be less than the natural recovery rate of the beach (McNinch and Wells, 1992; Tye, 1983) integrated over the whole summer season. These guidelines were followed during our laboratory experiments although it was difficult to estimate the natural recovery rate of the beach without monitoring previous summer seasons (on the prototype) or formerly testing experiments of the natural conditions (on the laboratory). Additionally, the recovery rate was found to depend on marine dynamics and change from one beach to another. This result indicates that it is necessary to monitor the evolution of beach profiles during summer before designing scraping actions on them.

The innovative NABE ploughing technique has proved to accelerate natural beach accretion in field experiments (Gainza et al., 2019), and in the laboratory at both a real scale (Pellón et al., 2023) and a reduced one (this study). The main advantages of the ploughing technique are: its easy design, the fact that it is inexpensive, it minimizes ecological disturbance, takes advantage of natural processes, and achieves wider dry beaches. Furthermore, the ploughing technique may be easily applied on beaches during routine daily cleaning operations. Due to the novelty of this technique, some questions are still to be answered in future studies, such as: *what is the effect of a spring storm acting over the ploughed bedforms?,* and, *is it possible to optimize the distance between consecutive ridges to enhance accretion even more and reduce the need for machinery?*

This study shows that the selection of the most appropriate NABE technique should be determined by the aim of each specific coastal management project. To achieve a wider dry beach the most appropriate techniques were either ploughing (PLOUGH) or scraping the low intertidal area filling the beach berm (L2BF) or scraping creating an intertidal bar (L2B). For dune nourishment or protection against winter storm purposes, the best solution is scraping, either the low or upper intertidal area (L2D or U2D), and using the sand for the nourishment of the subaerial area of the beach. Note that only low-energy marine conditions were tested in the laboratory. This means that the results obtained are only valid for NABE actions performed in the spring when fair weather is expected afterwards (during the spring and summer seasons).

Smutz et al. (1980) stated that, when carrying out a beach scraping, the flatter the nearshore profile, the larger the accretion. This statement has been confirmed in our experiment. Such relationship with the nearshore profile can be seen, for example, through a comparison of the L2D and U2D (channels 5 and 6). In U2D, the borrow area was located next to high tide level which caused a more dissipative beach profile during the high tide, while in L2D, the borrow area was located at the lower intertidal area and took the profile to more dissipative conditions only during mid-tide. During high tide, the water level stays almost stationary for longer periods than during mid-tide periods, when the water level changes rapidly. The longer duration of the wave action under the dissipative profile of U2D during high tide resulted in a stronger accretion effect. On the contrary, the short duration of dissipative conditions during mid-tide in L2D was not enough to obtain the same effectiveness in terms of accretion. Based on that, in places with a large tidal range, it is recommended to borrow the sediment from areas of the intertidal beach at the limit of the high tide level, in a way that more dissipative conditions are obtained during that tidal period.

Our experiments show that wave overtopping can cause an increase in berm height but not necessarily shoreline progradation. In nature, such processes frequently occur at the end of the summer season (September), when the wave period starts to grow and the wave runup increases. The accreted volume of sand generates a higher berm while beach width is preserved. It is important to highlight that a proper prediction of beach berm height is key for the success of NABE actions that intend to produce beach widening by placing the filling material on the beachfront (L2BF). By identifying the berm's height, it is possible to place the sediment just above the height of the future accretion berm and achieve an optimal use of the sediment to provide the maximum progradation of the shoreline. Fig. 10 shows a scheme of two non-optimal design possibilities. If the sediment is placed above the height of the future berm (where no waves will reach), this sand could be reshaped to the beachfront, widening the dry beach even more (Fig. 10b, 6k and 6l). On the other hand, without a proper estimate, the artificially generated berm may be placed below the current height level of the berm. In this case, the wave overtopping the berm will remove the sediment from the beachfront and place it over the berm, reducing progradation (Fig. 10c and 6j). In our experiments, we used the wave runup (computed with the slopes shown in Fig. 8) over high tide level as a proxy to estimate the water level that induces the formation of the berm and related it to berm height. Following this approach, our results showed that Stockdon's et al. (2006) runup formulation overpredicted berm height in Test A and C but fell below the resulting berm's height in Test B (see reference levels in Fig. 6). This can be explained by the fact that such formula was based on data from field experiments and some differences are expected when they are applied to scaled laboratory conditions (Gomes da Silva et al., 2020). However, despite the fact that the prediction did not match the resulting berm height perfectly, we consider that such values are accurate enough to be used as a first proxy estimate of berm height for scraping purposes on beaches. Obviously, more accurate formulations for the prediction of runup on reflective beaches are desirable for the design of beach scraping actions (note that this requires good estimates of the swash zone slope too).

Using sand from the borrow area to nourish the dune did not enhance progradation of the shoreline and further beach widening. However, such a technique may still be useful in areas where dune recovery is a priority. When sand is scraped for dune nourishment purposes, some aspects must be considered, such as dune design, space availability, and aeolian dynamics (Coastal Dune Management, 2001). Pellón et al. (2020) provided useful tools for the design of foredunes. The dune toe location and foredune volume can be determined as a function of local aeolian and marine conditions. Fencing and planting are also recommended, as the scraped sand may be removed and lost to offshore areas

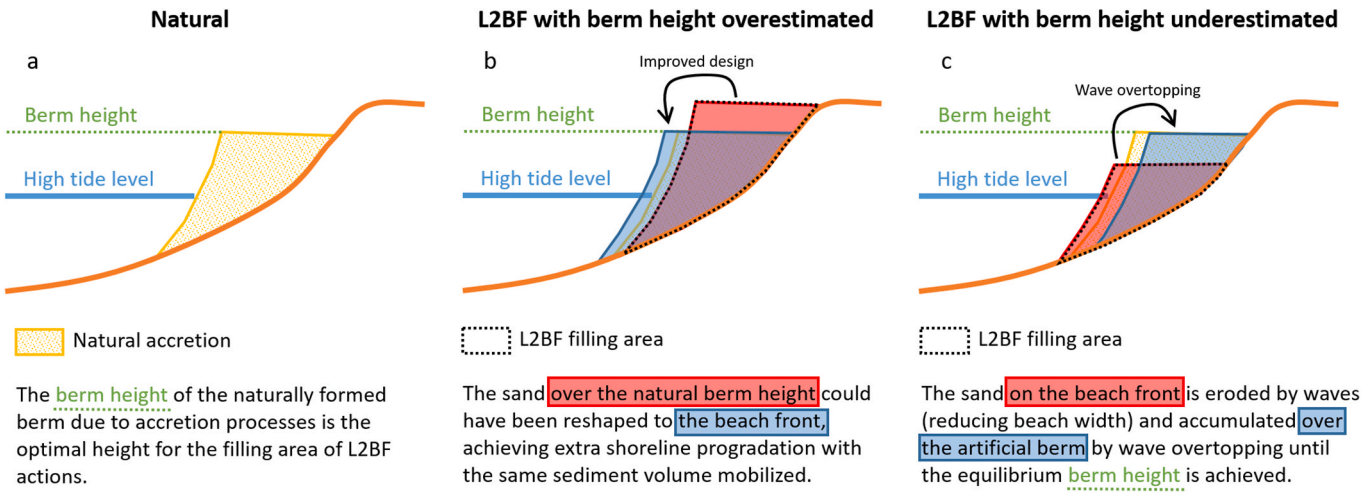

Fig. 10. Non-optimal design scheme of the L2BF filling area.

by future extreme wave events, or to inland areas through aeolian sediment transport (Conaway and Wells, 2005).

Another point to consider when applying beach scraping is the ecological impact of such a technique. The upper part of the intertidal area is a habitat for macrofauna, and also a foraging, nesting, and breeding location for avifauna and turtles (Dare, 2003; Govarets and Lauwerts, 2009). The intertidal area is a highly variable and dynamic environment that changes frequently due to wave and tidal action. Thus, the species that live in this environment are expected to be adapted to frequent changes and therefore able to recover quickly from disturbances (Batton, 2007). Additionally, recolonization processes are determined by the duration and intensity of the works. In this sense, the analysed techniques are a 'short-term pulse' disturbance (Speybroeck et al., 2006) and it is believed that species can recover more easily than under the effect of other hard-engineering solutions. Smith et al. (2011) assessed the impact of beach scraping on macroinvertebrates and did not find a detectable effect on biodiversity. Besides, a correct management of the beach can provide new habitats such as a healthy and stable beach and dune. Furthermore, some authors propose timing the actions to avoid turtle nesting periods (Crain et al., 1995) or effects on migratory species (Erskine and Thompson, 2003). Both aspects are site-specific and must be considered during NABE design. Further studies on the specific effect of scraping and ploughing actions over the entire ecosystem, from the submerged area to the dune, are still necessary to have a complete view of the ecological impact of these techniques.

Finally, it should be mentioned that the morphologic changes caused by the Test waves in the laboratory occurred fast, in a period of only 2 to 4 tidal cycles. This might have been caused by the low-density sediment used, as a scale effect. The reduced dimensionless fall velocity in the model compared to the prototype may accelerate beach accretion as well. Such a quick response of the sediment impeded the development of accretion speed comparisons between the various NABE techniques used in our experiments. This study only analysed beach width and accretion on the beach berm achieved at the maximum accretion state. The obtention of larger accretion volumes could be interpreted as the result of a faster accretion process once wave action begins, wider beaches being formed earlier in the summer by using these techniques. However, further research must be developed to ensure this desirable effect for touristic purposes.

5. Conclusions

The use of low-density synthetic sediment allowed the reduced scale simulation of a full beach profile under the simultaneous action of waves and tides. Five different Nature-Assisted Beach Enhancement (NABE) techniques were tested and their effectivity was determined by comparison to natural beach behaviour (control).

Beach berm geometry was mainly determined by marine dynamics. Incoming wave height and peak period conditioned berm height and swash zone slope with no effect from the NABE techniques on these variables. However, beach ploughing and scraping were related to shoreline position and dry beach width. When using these techniques, accretion volume was mainly determined by waves and the geometry of the berm, with variations due to the effect of NABE techniques. Generally speaking, the smaller the dimensionless fall velocity, the larger the accretion. Nevertheless, wave height and period may play a role, as Test A and C had similar dimensionless fall velocity, but for Test C the accretion could have been reduced by the low energy of the simulated waves.

The recommended NABE technique depends on the objective. For beaches where a wider dry beach is sought, the recommended actions are ploughing or scraping, borrowing the sand from the low intertidal area and filling an intertidal bar or the beachfront (with a careful design of the berm geometry) during spring. For beaches where inland protection from erosion and flooding under winter storms is sought, the recommendation is borrowing sand from the intertidal area during spring (and preferably from the upper intertidal area) and nourishing the dune or the upper dry beach, where the sediment will be available to buffer the erosion caused by winter storms.

Ploughing the intertidal area at each low tide demonstrated to be an effective technique to enhance beach accretion and achieve a wider dry beach. The combined effect of waves and tides makes ploughing effective and easy to apply.

The creation of an intertidal bar by scraping the low intertidal area resulted in wider dry beaches. The sediment on the intertidal bar was partially accreted to the beach berm and partially eroded offshore.

The generation of a berm by the scraping technique may produce wider beaches if adequately designed. The geometry of the berm generated by "machinery" highly influenced the results. The berm height and swash zone slope should match the naturally formed berm due to accretion. These berm's geometric characteristics are difficult to predict as they depend on marine dynamics and they evolve throughout the summer season. The placement of sediment on the berm reduces the disequilibrium that triggers accretion and therefore the sediment volume that is naturally moved onshore is reduced. Additional research on the impact of berm geometry on accretion and dry beach width is required.

The recommended borrow area for dune nourishment is the upper part of the intertidal area. The beach profile becomes more dissipative at high tide and this leads to more disequilibrium between actual and

equilibrium geometries, increasing onshore sediment transport and achieving larger accretion volumes.

Further studies are needed to determine if NABE techniques can result in wider beaches as of the beginning of the touristic summer season or only at the maximum accretion state as was demonstrated in this study.

CRediT authorship contribution statement

E. Pellón: Methodology, Investigation, Formal analysis, Validation, Data curation, Writing – Original Draft, Writing – Review & Editing, Visualization, Project administration. C. Vidal: Investigation, Supervision, Conceptualization, Methodology, Writing – Original Draft, Writing – Review & Editing. P. Gomes: Methodology, Writing – Review & Editing. I. Aniel-Quiroga: Methodology, Writing – Review & Editing. M. González: Supervision, Conceptualization, Funding acquisition, Project administration, Methodology, Resources, Writing – Review & Editing. R. Medina: Supervision, Conceptualization, Methodology, Writing – Review & Editing.

Declaration of competing interest

The authors declare that they have no known competing financial interests or personal relationships that could have appeared to influence the work reported in this paper.

Data availability

Data will be made available on request.

Acknowledgements

The Beach-ART project is funded by the Spanish Ministry of Economy, Industry, and Competitiveness under grant BIA2017-89491-R. The authors acknowledge the financial support from the Government of Cantabria through the Fénix Programme. We also acknowledge the financial support from the Contract Program of the Government of Cantabria – Universidad de Cantabria through the project Hybrid shoreline evolution model for long-term scales integrating longshore and cross-shore processes. The authors are grateful for the technical assistance of all the laboratory personnel during the experiments.

APPENDIX I

The scale of a magnitude M (λ_M) is defined here as the ratio between the value of this magnitude in the prototype, M_p, and the corresponding value in the model, M_m, as shown in equation (3):

$$\lambda_M = \frac{M_p}{M_m} \tag{3}$$

The Kinematics of free surface flows are mostly controlled by gravity. If in Newton's 2nd law, the inertial forces (F_i) are divided by the gravitatory ones (F_g), the non-dimensional expression corresponding to gravity forces is called the Froude number, see equation (4).

$$F_n = \frac{F_i}{F_g} = \frac{L}{gT^2} \tag{4}$$

where g is the acceleration of gravity, T is a magnitude of time and L is length. In the case of gravity wave flows, the correct scaling of the processes of shoaling, refraction and diffraction implies the use of non-distorted models, so the length scale λ_l should be applied to the three spatial dimensions. The similarity between the Froude number in the flow of the prototype and that of the model (sub-indexes p and m, respectively), $\lambda_F = \frac{F_p}{F_m} = 1$ implies that the time and velocity scales are the square root of the length scale, equation (5):

$$\lambda_t = \lambda_V = \sqrt{\lambda_l} \tag{5}$$

Bed load sediment transport of non-cohesive sands under waves and currents is mainly controlled by the following dimensional variables.

- d_{50}: Median sediment grain size
- ρ_s: Sediment grain density
- ρ_w: Water density
- ν: Water kinematic viscosity
- u_*: Bottom friction velocity

If u_*, ρ_w and d_{50} are assumed as fundamental variables, the application of the π-Buckingham theorem (1914) produces the non-dimensional expressions indicated in equations (6) and (7).

$$R_{e^*} = \frac{u_* d_{50}}{\nu} \tag{6}$$

$$\theta = \frac{\rho_w u_*^2}{(\rho_s - \rho_w) g d_{50}} = \frac{\tau_0}{(\rho_s - \rho_w) g d_{50}} \tag{7}$$

where (in (7)), τ_0 is bed shear stress. Equation (6) is the grain Reynolds number (R_{e^*}) and controls the shape of the bottom boundary layer, i.e. the tension of the flow over the sediment grains. Equation (7) is the Shields (1936) number (Θ) and controls the initiation of motion of the sediment.

If the movable bed experiments are carried out assuming that the Shields number in the prototype and model are equal, then the scale of the Shields number should be equal to 1, equation (8):

$$\lambda_\theta = \frac{\theta_p}{\theta_m} = 1 \tag{8}$$

Under the wave's oscillatory motion, the peak bed shear stress can be expressed in terms of the orbital velocity amplitude on top of the bottom boundary layer, U_δ, using a wave friction factor, f_w, as in equation (9):

$$\tau_0 = \frac{1}{2}\rho_w f_w U_\delta^2 \tag{9}$$

Soulsby (1997) proposed expression (10) for the wave friction factor in terms of the bottom orbital excursion, A_b, and Nikuradse's equivalent sand grain roughness, k_s.

$$\mathrm{f_w} = 0.237\left(\frac{A_b}{k_s}\right)^{-0.52} \tag{10}$$

Assuming the conventional value $k_s = 2.5\ d_{50}$, (Nielsen, 1992), and for shallow waters $A_b = (U_\delta T_p)/(2\pi)$, equation (11) is obtained.

$$f_w = 0.993\left(\frac{d_{50}}{U_\delta T_p}\right)^{0.52} \tag{11}$$

where in (11) T_p is sea state peak period.

Using the wave friction factor of (11) and the expression (9) of the bed shear stress, the Shields number takes the form of equation (12).

$$\theta = \frac{0.496\mathrm{U_\delta^2}\left(\frac{d_{50}}{\mathrm{U_\delta T_p}}\right)^{0.52}}{\Delta g d_{50}} \tag{12}$$

where in (12), Δ is the sediment's relative submerged density, $\Delta = \frac{(\rho_s - \rho_w)}{\rho_w}$.

Using expression (12) and expression (8) to calculate the similarity of the Shields number, and taking into account the Froude scale for time and velocity of equation (5) and that $\lambda_g = 1$ (the gravity acceleration is the same in the prototype and the model), the following expression (13) for the relationship between the length, sediment relative density and grain size scales is obtained.

$$\lambda_d = \frac{\lambda_l}{\lambda_\Delta^{2.083}} \tag{13}$$

If the movable bed experiments are carried out assuming the similarity of the grain Reynolds number, then the scale of the grain Reynolds number should be equal to 1, equation (14).

$$\lambda_{Re^*} = \frac{R_{e^*p}}{R_{e^*m}} = 1 \tag{14}$$

Using (7) we can state that $u_* = (\tau_0/\rho_w)^{1/2}$ and the equations for bottom shear stress (9) and bottom friction factor (11), applied to equation (6) lead to the following equation (15) for the grain Reynolds number.

$$\mathrm{R_{e^*}} = \frac{0.704\mathrm{U_\delta}\left(\frac{d_{50}}{\mathrm{U_\delta T_p}}\right)^{0.26} d_{50}}{\nu} \tag{15}$$

Using expression (15) and equation (14) to achieve the similarity of the grain Reynolds number and taking into account the Froude scale for flow velocity and time, the relationship (16) between the scales of length, grain size and fluid kinematic viscosity is obtained.

$$\lambda_d = \lambda_\nu^{0.794}\lambda_l^{-0.19} \tag{16}$$

Equations (13) and (16) establish the relationships between the sediment relative density scale, the grain size scale and the length scale that should be taken into account for bed load transport similarity in physical experiments.

In the surf zone of beaches, suspended load transport is also fundamental to describe sediment transport. For a correct description of this transport, besides the variables involved in the Shields and grain Reynolds numbers, the significant wave height, H_s, and the fall velocity of grain particles, w, are determinant. The fall velocity of grain particles depends on grain size and density, as well as on water viscosity, so the only new variable involved is wave height. The most used non-dimensional equation that takes into account this new variable is the dimensionless fall velocity, Ω, (Dean, 1973; Gourlay, 1968) given in (17).

$$\Omega = \frac{H_s}{w\ T_p} \tag{17}$$

The dimensionless fall velocity has also been used to explain different beach states (Masselink and Short, 1993; Wright and Short, 1984). Values of Ω higher than 6 correspond to dissipative beaches and those lower than 2 to reflective beaches. Values between 2 and 6 correspond to intermediate beaches that develop longitudinal and transversal bars.

Using equation (17) and taking into account Froude's scale for flow velocities and time, the scale of the dimensionless fall velocity is given by equation (18) as a function of the length and the fall velocity of grain particles scales.

$$\lambda_\Omega = \frac{\lambda_l^{0.5}}{\lambda_w} \tag{18}$$

Another non-dimensional number that is used to discriminate between bed load and suspended load transport is the Rouse number (R_o), which gives a relationship between the fall velocity of grain particles and the friction velocity, equation (19).

$$R_o = \frac{w}{\kappa u^*} \tag{19}$$

where, in (19), κ is the von Karman constant. The load transport modes in terms of the Rouse number are given by (Whipple, 2004).

- $R_o > 2.5 \rightarrow$ Bed load
- $1.2 \leq R_o \leq 2.5 \rightarrow$ 50% suspended load
- $0.8 \leq R_o < 1.2 \rightarrow$ 100% suspended load
- $R_o < 0.8 \rightarrow$ Wash load

Using equations ((7), (9), (11) and (19) the scale of the Rouse number can be expressed as (20):

$$\lambda_{Ro} = \frac{\lambda_w}{\lambda_d^{0.26}\lambda_l^{0.24}} \tag{20}$$

The problem with the use of the Ω or R_o numbers to obtain the similarity of suspended transport in small-scale experiments is that the fall velocity of grain particles depends on the falling flow regime (laminar, transition or turbulent). As the prototype and model grains can fall into different flow regimes this gives 6 different possible scales. Hallermeier (1981) proposed the parameter A to discriminate between the different regimes (equation (21), (22), (23), and (24)).

$$\mathrm{A} = \frac{\Delta g {d_{50}}^3}{\nu^2} \tag{21}$$

The proposed fall velocities for the different fall regimes are:

$$\text{Laminar} : \mathrm{A} \leq 39;\ \mathrm{w} = \frac{\Delta g {d_{50}}^2}{18\nu} \tag{22}$$

$$\text{Transition} : 39 < \mathrm{A} < 10^4; \mathrm{w} = \frac{(\Delta g)^{0.7} {d_{50}}^{1.1}}{6\nu^{0.4}} \tag{23}$$

$$\text{Turbulent} : \mathrm{A} \geq 10^4; \mathrm{w} = \frac{(\Delta g)^{1/12} {d_{50}}^{0.5}}{0.91} \tag{24}$$

In this study, the model's sediment properties (grain size and density) are obtained from Shields and grain Reynolds numbers' similarities and the scales of the Ω and R_o numbers are derived quantities. The dissimilarity in these two parameters between the model and the prototype has implications that will be discussed further in this study.

The length scale applied in the experiments conducted in this study, $\lambda_l = 8$ was determined by the capabilities and size of the wave tank where the model was built. Other known parameters and resulting scales are given in Table 3.

The characteristics of the prototype and the freshwater used in the model are known. The scale relation (16) obtained for the similarity of the grain Reynolds number allows the determination of the targeted sediment grain size. Then, the scale relation (13) obtained for the similarity in the Shields number, determines the relative submerged density scale and therefore the target sediment density. The target values obtained from the Froude, Shields and grain Reynolds numbers similarities are summarized in Table 3.

The density of the sediment used for physical models is restricted by the densities of available materials. In this study, we used synthetic sediment which was very similar to the targeted one (i.e. plastic blast of density $\rho_s = 1\,500\ \mathrm{kg/m^3}$, gradation 40/60, mean grain size $d_{50} = 0.37$ mm, and porosity of 0.5, see Table 3). With this sediment, the prototype and model regimes of fall velocity, equation (21), are in the transition region and the fall velocity of grain particles can be calculated using equation (23), see Table 3.

The resulting scales of the five non-dimensional parameters are.

- Froude number (flow variables imposed in the wave tank): $\lambda_F = 1$
- Shields number, equation (12): $\lambda_\theta = 0.997 \cong 1$
- Grain Reynolds number, equation (15): $\lambda_{Re^*} = 1.034 \cong 1$
- Fall velocity parameter scale (Dean), equation (17): $\lambda_\Omega = 1.835$
- Rouse number scale, equation (19): $\lambda_{Ro} = 1.016 \cong 1$

As shown, with the model sediment chosen for the experiments, all parameters (Froude, Shields, Reynolds grain and Rouse) were similar in the prototype and the model. The dimensionless fall velocity however was higher in the prototype than in the model, meaning that the modelled beach would tend to be more reflective than the prototype. According to the beach classification based on Ω (Wright and Short, 1984), and also accounting for the relative tidal range (Masselink and Short, 1993), the beach in the model evolves from longshore bar-through (LBT) to low tide terrace (LTT) beach state, while in the prototype it evolves from dissipative (D) to LTT. Therefore, the difference induced by the non-similarity of the fall velocity parameter is that the initial state is dissipative in the prototype and LBT in the model. Both initial beach states (D and LBT) form two-dimensional beaches. The main differences are that the dissipative beach has a longer breaking zone, a larger distance to the first bar, through of the bar less marked, less slope of the beachfront and breaking zones, and spilling breaking (instead of plunging). These differences do not affect the goal of determining which of the NABE techniques is more effective for enhancing beach recovery. The experiments performed are representative of the evolution of a beach from post-storm conditions (even in nature the beach may not achieve a dissipative sea state due to the short duration of spring marine storms) to calm summer weather conditions.

The relatively large size of the grains of the synthetic sediment produces scale effects on the bed roughness and therefore the bottom friction. Consequently, the variation of wave height per unit of length is around 3 times bigger in the model than in the prototype in the shoaling zone. This scale effect becomes negligible in the breaking zone, where wave dissipation due to breaking is much bigger than bottom dissipation.

Table 3
Prototype, target and physical model variables and scales for sediment and water. (1) Known values; (2) Target values obtained from Froude, Shields and Reynolds numbers similarities; (3) Final model sediment variables and scales used in the physical experiments.

	Variable	Symbol	Value	Units
(1) Known values	Prototype sediment density	ρ_{sp}	2 650	kg/m^3
	Prototype sediment grain size	d_{50p}	0.270	mm
	Prototype sediment relative submerged density	Δ_p	1.583	–
	Prototype fall velocity of grain particles	w_p	0.0313	m/s
	Prototype water density (salt water)	ρ_{wp}	1 026	kg/m^3
	Prototype water kinematic viscosity (salt water)	ν_p	$1.223\ 10^{-6}$	m^2/s
	Model water density (freshwater)	ρ_{wm}	1 000	kg/m^3
	Model water kinematic viscosity (freshwater)	ν_m	$1.141\ 10^{-6}$	m^2/s
	Water density scale	$\lambda_{\rho w}$	1.026	–
	Water kinematic viscosity scale	λ_ν	1.072	–
(2) Target values	Target sediment grain size scale, equation (16)	λ_{dt}	0.712	–
	Target sediment density scale	$\lambda_{\rho st}$	1.771	–
	Target sediment relative submerged density scale, equation (13)	$\lambda_{\Delta t}$	3.194	–
	Resulting fall velocity of grain particles scale	λ_{wt}	1.512	–
	Target sediment grain size	d_{50t}	0.379	mm
	Target sediment relative submerged density	Δ_t	0.496	–
	Target sediment density	ρ_{st}	1 496	kg/m^3
	Resulting fall velocity of grain particles	w_t	0.0207	m/s
(3) Final model values	Model sediment grain size	d_{50m}	0.370	mm
	Model sediment relative submerged density	Δ_m	0.500	–
	Model sediment density	ρ_{sm}	1 500	kg/m^3
	Model fall velocity of grain particles	w_m	0.0203	m/s
	Model sediment grain size scale	λ_d	0.730	–
	Model sediment density scale	$\lambda_{\rho s}$	1.767	–
	Model sediment relative submerged density scale	λ_Δ	3.166	–
	Model fall velocity of grain particles scale	λ_w	1.542	–

References

Alsina, J.M., Cáceres, I., Brocchini, M., Baldock, T.E., 2012. An experimental study on sediment transport and bed evolution under different swash zone morphological conditions. Coast. Eng. 68, 31–43. https://doi.org/10.1016/j.coastaleng.2012.04.008.

Aubrey, D.G., 1979. Seasonal patterns of onshore/offshore sediment movement. J. Geophys. Res. 84, 6347–6354.

Baldock, T.E., Alsina, J., 2013. Impact of beach scraping on near shore sediment transport and bar migration. Coasts Ports 35–40, 2013.

Batton, R., 2007. Tidal fish habitats, erosion control and beach replenishment. Queensl. Dep. Prim. Ind. Fish.

Bruun, P., 1983. Beach scraping. Coast. Eng. 7, 167–173.

Carley, J.T., Shand, T.D., Coghlan, I.R., Blacka, M.J., Cox, J., Littman, A., Fitzgibbon, B., Mclean, G., Watson, P., 2010. Beach scraping as a coastal management option. 19th NSW Coast. Conf. 1–20.

Coastal Dune Management, 2001. NSW Dep. L. Water Conserv.

Conaway, C.A., Wells, J.T., 2005. Aeolian dynamics along scraped shorelines, Bogue Banks, North Carolina. J. Coast Res. 21, 242–254. https://doi.org/10.2112/01-089.1.

Crain, D.A., Bolten, A.B., Bjorndal, K.A., 1995. Effects of beach nourishment on sea turtles: review and research initiatives. Restor. Ecol. 3, 95–104. https://doi.org/10.1111/J.1526-100X.1995.TB00082.X.

Dare, J.L., 2003. Alternative shore protection strategies: innovative options and management issues. Proj. Rep. Submitt. to Mar. Resour. Manag. Progr. Coll. Ocean. Atmospleric Sci. Oregon State Univesity Partial fulfilment Requir. degree Master Sci. 91.

Dean, R.G., 1973. Heuristic models of sand transport in the surf zone. Proc. Conf. Eng. Dyn. Surf Zo. 208–214.

Erskine, A., Thompson, M., 2003. New Brighton Vegetation Management Plan. Enviromnental Train. Employ. Inc. EnviTE NSW.

Gainza, J., Garnier, R., Nuñez, P., Jaramillo, C., González, E.M., Medina, R., Liria, P., Epelde, I., Uriarte, A., Monge-Ganuzas, M., 2019. Accelerating beach recovery by plowing the intertidal bar: a field experiment along the northern Spanish coast. J. Coast Res. 35, 973. https://doi.org/10.2112/jcoastres-d-18-00033.1.

Gallagher, E.L., Elgar, S., Guza, R.T., 1998. Observations of sand bar evolution on a natural beach. J. Geophys. Res. Ocean. 103, 3203–3215.

Gomes da Silva, P., Coco, G., Garnier, R., Klein, A.H.F., 2020. On the prediction of runup, setup and swash on beaches. Earth Sci. Rev. https://doi.org/10.1016/j.earscirev.2020.103148.

Gordon, A.D., 2015. When did you last NABE a beach – beach scraping demystified for fun and profit. Proc. 24st NSW Coast. Conf. Forster, NSW, Novemb. 1–10, 2015.

Gourlay, M.R., 1968. Beach and Dune Erosion Tests. Deltares (WL).

Govarets, A., Lauwerts, B., 2009. Assessment of the impact of coastal defence structures. OSPAR Comm. Belgium 29.

Grasso, F., Michallet, H., Barthélemy, E., Certain, R., 2009. Physical modeling of intermediate cross-shore beach morphology: transients and equilibrium states. J. Geophys. Res. Ocean. 114, 1–15. https://doi.org/10.1029/2009JC005308.

Guannel, G., Özkan-Haller, H.T., Haller, M.C., Kirby, J.T., 2007. Influence of velocity moments on sand bar movement during CROSSTEX. In: Coastal Sediments '07, pp. 28–41. ASCE.

Hallermeier, R.J., 1981. Terminal settling velocity of commonly occurring sand grains. Sedimentology 28, 859–865. https://doi.org/10.1111/j.1365-3091.1981.tb01948.x.

Hamm, L., Capobianco, M., Dette, H.H., Lechuga, A., Spanhoff, R., Stive, M.J.F., 2002. A summary of European experience with shore nourishment. Coast. Eng. 47, 237–264. https://doi.org/10.1016/S0378-3839(02)00127-8.

Hasselmann, K., Barnett, T.P., Bouws, E., Carlson, H., Cartwright, D.E., Enke, K., Ewing, J.A., Gienapp, H., Hasselmann, D.E., Kruseman, P., Meerburg, A., Müller, P., Olbers, D.J., Richter, K., Sell, W., Walden, H., 1973. Measurements of Wind-Wave Growth and Swell Decay during the Joint North Sea Wave Project (JONSWAP). Deutches Hydrographisches Institut.

Hughes, S.A., 1984. Tma shallow-water spectrum: description and applications. Tech. Rep. CERC (US Army Eng. Waterw. Exp. Station. Coast. Eng. Res.

Kraus, N.C., Larson, M., Kriebel, D.L., 1991. Evaluation of beach erosion and accretion predictors. Am. Soc. Civ. Eng. 572–587.

Larsen, B.E., van der A, D.A., Carstensen, R., Carstensen, S., Fuhrman, D.R., 2023. Experimental investigation on the effects of shoreface nourishment placement and timing on long-term cross-shore profile development. Coast. Eng. 180, 104258 https://doi.org/10.1016/j.coastaleng.2022.104258.

Luijendijk, A., Hagenaars, G., Ranasinghe, R., Baart, F., Donchyts, G., Aarninkhof, S., 2018. The state of the world's beaches. Sci. Rep. 1–11. https://doi.org/10.1038/s41598-018-24630-6.

Masselink, G., Short, A.D., 1993. The effect of tide range on beach morphodynamics and morphology: a conceptual beach model. J. Coast Res. 9, 785–800.

McGranahan, G., Balk, D., Anderson, B., 2007. The rising tide: assessing the risks of climate change and human settlements in low elevation coastal zones. Environ. Urbanization 19, 17–37. https://doi.org/10.1177/0956247807076960.

McNinch, J.E., Wells, J.T., 1992. The effectiveness of beach scraping as a method of erosion control. Shore Beach 60, 13–20.

Monge-Ganuzas, M., Gainza, J., Liria, P., Epelde, I., Uriarte, A., Garnier, R., González, M., Nuñez, P., Jaramillo, C., Medina, R., 2017. Morphodynamic evolution of Laida beach (Oka estuary, Urdaibai Biosphere Reserve, southeastern Bay of Biscay) in response to supratidal beach nourishment actions. J. Sea Res. 130, 85–95. https://doi.org/10.1016/j.seares.2017.06.003.

Nielsen, P., 1992. Coastal Bottom Boundary Layers and Sediment Transport, Advanced Series on Ocean Engineering. WORLD SCIENTIFIC. https://doi.org/10.1142/1269.

Pellón, E., Aniel-Quiroga, I., González, M., Medina, R., Vidal, C., 2023. Working with nature to enhance beach accretion: laboratory experiments of beach ploughing. Coast. Eng. 180 https://doi.org/10.1016/j.coastaleng.2022.104267.

Pellón, E., de Almeida, L.R., González, M., Medina, R., 2020. Relationship between foredune profile morphology and aeolian and marine dynamics: a conceptual model. Geomorphology 351, 106984. https://doi.org/10.1016/j.geomorph.2019.106984.

Sánchez-González, J.F., Martín-Hidalgo, M., de la Peña Olivas, J.M., 2017. Ensayo en Modelo Físico a Gran Escala de las Operaciones de Reperfilado de Playas para la Protección del Territorio frente a Temporales de Oleaje. In: XIV Jornadas Españolas de Costas y Puertos.

Shields, A., 1936. Application of similarity principles and turbulence research to bed-load movement. Soil Conserv. Serv. 47.

Short, A.D., 1991. Macro-meso tidal beach morphodynamics - an overview. J. Coast Res. 7, 417–436.

Smith, S.D.A., Harrison, M.A., Rowland, J., Fitzgibbon, B.E., 2011. Assessing the impacts of beach scraping on the macroinvertebrates of new brighton beach, northern NSW. In: Aust. Coast. Soc. Ltd.; 20th New South Wales Coast. Conf. (Tweed Heads, NSW), pp. 1–13.

Smutz, M., Griffith, J.W., Yu-Hwa, W., 1980. Nature assisted beach enhancement or sisyphus vs zeus. Shore Beach 32–36.

Soulsby, R., 1997. Dynamics of Marine Sands, Dynamics of Marine Sands. Thomas Telford Ltd. https://doi.org/10.1680/DOMS.25844.

Speybroeck, J., Bonte, D., Courtens, W., Gheskiere, T., Grootaert, P., Maelfait, J.P., Mathys, M., Provoost, S., Sabbe, K., Stienen, E.W.M., Van Lancker, V., Vincx, M., Degraer, S., 2006. Beach nourishment: an ecologically sound coastal defence alternative? A review. Aquat. Conserv. Mar. Freshw. Ecosyst. 16, 419–435. https://doi.org/10.1002/aqc.733.

Stockdon, H.F., Holman, R.A., Howd, P.A., Sallenger, A.H., 2006. Empirical parameterization of setup, swash, and runup. Coast. Eng. 53, 573–588. https://doi.org/10.1016/j.coastaleng.2005.12.005.

Tye, R.S., 1983. Impact of hurricane David and mechanical dune restoration on folly beach, South Carolina. Shore Beach 51, 3–9.

Whipple, K., 2004. Surface Processes and Landscape Evolution [WWW Document]. MIT OpenCourseWare 12.163. URL. https://ocw.mit.edu/courses/12-163-surface-processes-and-landscape-evolution-fall-2004/pages/lecture-notes/, 3.9.23.

Wright, L.D., Short, A.D., 1984. Morphodynamic variability of surf zones and beaches: a synthesis. Mar. Geol. 56, 93–118. https://doi.org/10.1016/0025-3227(84)90008-2.

Yoo, H.J., Kim, H., Lee, J.L., Park, J.Y., 2021. Asymmetry between accretional advance and erosional retreat of shoreline position in on-offshore direction. J. Coast Res. 114, 6–10. https://doi.org/10.2112/JCR-SI114-002.1.